Prediction and control of spin polarization in a Weyl semimetallic phase of BiSb

Sobhit Singh,[1,][*] A. C. Garcia-Castro,[1,2,3] Irais Valencia-Jaime,[1,2] Francisco Muñoz,[4,5] and Aldo H. Romero[1,][†]

[1]*Department of Physics and Astronomy, West Virginia University, Morgantown, West Virginia 26505-6315, USA*
[2]*Centro de Investigación y Estudios Avanzados del IPN, MX-76230 Querétaro, México*
[3]*Physique Théorique des Matériaux, Université de Liège, B-4000 Sart-Tilman, Belgium*
[4]*Departamento de Física, Facultad de Ciencias, Universidad de Chile, Casilla 653, Santiago, Chile*
[5]*Centro para el Desarrollo de la Nanoscience y la Nanotechnología CEDENNA, Santiago, Chile*

By means of first-principle calculations, we report a stoichiometric crystal structure of BiSb with broken space-inversion symmetry. This structure is insulating in bulk and has nontrivial band topology. We observe a pressure driven Weyl semimetallic electronic phase transition in this BiSb system without a crystal phase change. The obtained Weyl semimetallic phase exists in the 4.0–6.0 GPa pressure range. We find that a total of 12 pairs of Weyl points, 12 monopoles and 12 antimonopoles, exist in the Brillouin zone. Additionally, the spin texture of the bulk BiSb compound appears to be electrically controllable when the interlink between pressure and an electric field is exploited. This produces novel manipulable topological transport properties in this system.

Weyl fermions have recently attracted the attention of researchers due to their unique intriguing physical properties such as the presence of discontinuous Fermi arcs [1–4], quantized anomalous Hall effect [5,6], quantum transport [7], anomalous magnetoresistance [8], etc. In condensed matter systems, Weyl fermions can be realized as low-energy excitations near the touching points of two nondegenerate bands at discrete **k** points in the momentum space of a bulk system. These gapless band touching points are known as Weyl nodes or Weyl points [2]. Close to a Weyl point, bands have linear dispersion in all directions in **k** space. Each Weyl point can be characterized by an associated chirality or topological charge, which corresponds to a monopole or antimonopole of Berry curvature in momentum space.

In recent years, many different theoretical proposals have been reported for realization of Weyl semimetallic (WSM) phase in inversion (I)-symmetric [1,9–11] and I-asymmetric systems [12–21]. Several groups have recently reported the experimental realization of WSM phase in single crystal compounds [22–25] and in photonic crystals [26]. To the best of our knowledge, there is no report of controllable WSM phase in a stable compound. However, ferroelectric-like polar WSM compounds having large spin-orbit coupling (SOC) could open a new avenue of realization of novel transport properties. When we combine SOC with ferroelectricity, we obtain a class of novel multifunctional materials, called ferro-electric Rashba semiconductors (FERSC) [27]. Recently, S. Picozzi *et al.* have theoretically demonstrated the possible control and switching of the spin texture by means of an electric field in GeTe [27,28]. This prediction was later experimentally corroborated [29]. Furthermore, the recent experimental discovery of ferroelectric metals has generated huge interest in polar materials [30,31]. The interplay between SOC and polarity could yield exotic quantum phenomenon in polar ferroelectric metals [32,33]. Here, we take advantage of the large SOC of Bi and Sb atoms [34–37] and the ferroelectric

polarization of BiSb semiconductor to control the spin-related properties in the present BiSb system.

The $Bi_{1-x}Sb_x$ alloys are the first generation topological insulator [38]. In 2013, Kim *et al.* reported experimental evidence of WSM phase in $Bi_{1-x}Sb_x$ alloys for $x = 3\%$ by magnetoresistance measurements [8]. In the present work, we report a stoichiometric crystal structure of BiSb with broken I symmetry. This structure belongs to the space group 160 ($R3m$) and has nontrivial band topology. By means of first-principle calculations, we observe a pressure-induced WSM phase transition in the present BiSb system in 4.0–6.0 GPa pressure range. We have further exploited the coupling between pressure and electric field to realize and control the chirality of Weyl points in BiSb.

We used the projected augmented wave (PAW) method implemented in the VASP code to perform all density functional theory (DFT)-based first-principle calculations [39,40]. For all calculations presented in this Rapid Communication, we used a conventional unit cell of BiSb (space group 160: $R3m$), containing three atoms of Bi and three atoms of Sb [41]. The cell was relaxed, first in the internal coordinates and then in the volume until the total energy difference between two consecutive steps was smaller than 10^{-8} eV and the total residual forces were less than 10^{-5} eV/Å. Spin-orbit interaction was included for all ionic relaxations. For all pressure dependent electronic structure calculations, we employed isotropic pressure ranging from 1 to 10 GPa on the original unit cell. Further computational details are given in the Supplemental Material [42].

In the $R3m$ space group, BiSb has a layered crystal structure with alternative layers of Bi and Sb atoms oriented along the c axis of the rhombohedral unit cell [see crystal structure in Fig. 3(a)]. Lattice parameters of the fully relaxed unit cell are $a = b = 4.51$ Å, $c = 11.92$ Å, which are in good agreement with the experimental data [43]. To study the dynamical stability of BiSb, we performed phonon calculations using density functional perturbation theory (DFPT) as implemented in the ABINIT code [44–46]. We used different approximations for the exchange-correlation functional (LDA, LDA+SOC, PBE, and PBE+SOC) to compute phonon modes at different values of applied pressure. We found that BiSb in the $R3m$

———————
[*]Corresponding author: smsingh@mix.wvu.edu
[†]Corresponding author: Aldo.Romero@mail.wvu.edu
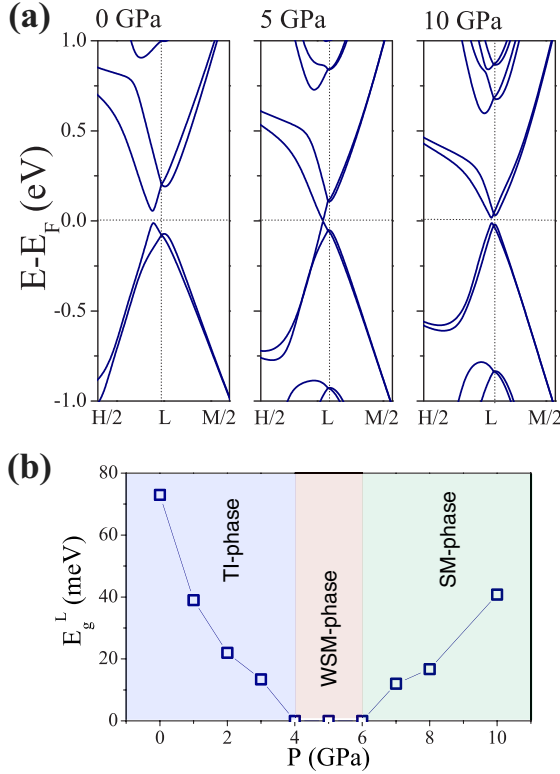
FIG. 1. (a) represents the evolution of the electronic band structure (with SOC) for different values of applied isotropic pressure, $P = 0.0$, 5.0, and 10.0 GPa. (b) depicts change in the direct electron band gap along the $H/2 \rightarrow L$ direction as a function of applied pressure, P.

phase is thermally and mechanically stable up to 10 GPa. Additional details regarding crystal structure, phonons, and elastic constants calculations are given in the Supplemental Material. This structure has already been experimentally synthesized due to its novel thermoelectric properties at low temperatures [43,47].

The electronic band-structure calculations (given in the Supplemental Material) reveal that without SOC, BiSb is an indirect band-gap semiconductor with indirect energy gap of 0.16 eV. The direct band gap is located at the L point of the hexagonal Brillouin zone. In the presence of SOC, each band of BiSb shows spin splitting. However, the spin degeneracy of bands still exits at the L point (Kramers' point), which confirms that BiSb breaks the I symmetry but preserves the time-reversal (TR) symmetry [Fig. 1(a)]. For TR-symmetric systems, lack of I symmetry is an essential requirement for realization of the WSM phase. We also notice that the SOC-induced band inversion takes places along the $H \rightarrow L$ direction. Such a band-inversion process yields topologically protected conducting surface states in the bulk insulating system. Thus, the band-structure calculations exhibit the nontrivial topological nature of bands in the BiSb system.

According to the theoretical model proposed in Refs. [12,48], one can possibly realize a gapless WSM phase by varying a control parameter m in the effective model Hamiltonian $H(\mathbf{k},m)$ of a bulk insulating system. For I-asymmetric systems, the gapless WSM phase exists for a finite range of the control parameter m. In the present work, we use

isotropic pressure (P) as the control parameter to tune the bulk band gap. Figure 1(a) shows the evolution in the direct band gap along the $H \rightarrow L$ direction for different values of applied pressure. The direct band gap along the $H \rightarrow L$ direction (E_g^L) decreases as we increase pressure up to 3.0 GPa [Fig. 1(b)]. Interestingly, with a further increase in pressure, E_g^L becomes zero at 4.0 GPa pressure and remains zero until 6.0 GPa. In this pressure range, the conduction band bottom (CBB) and the valence band top (VBT) accidentally touch each other along the $H \rightarrow L$ direction [see Fig. 1(a) for the 5.0 GPa case]. The dispersion of the bands close to the band touching point is linear in $\mathbf{k}$ and the band touching point is not located at any Kramers' points or along any high-symmetry direction of the bulk Brillouin zone. These facts give us signatures of a Weyl semimetallic phase in a 4.0–6.0 GPa pressure range. When we further increase the external pressure, we observe that the direct band gap E_g^L reopens. However, the system becomes semimetallic (SM) due to crossing of the Fermi level by other topologically trivial bands (Supplemental Material, Fig. S4). Thus, a pressure induced nontrivial insulator-WSM-semimetal phase transition takes place in the present BiSb system. A similar pressure induced phase transition has been reported for trigonal Te and Se systems [18].

Figure 2(a) shows the projection of spin components (S_x, S_y, and S_z) on the electronic bands for 5.0 GPa applied pressure. We observe similar behavior of spin projections for other values of P ($4.0 \leqslant P \leqslant 6.0$). Here, we have chosen the (001) direction as the quantization axis for all spin dependent calculations. In Fig. 2(a), we calculate the band structure along two different directions in $\mathbf{k}$ space: $H/2 \rightarrow L \rightarrow H'/2$ and $P/2 \rightarrow L \rightarrow Q/2$ [see Fig. 2(c) for directions]. Along the $H/2 \rightarrow L \rightarrow H'/2$ direction, one can clearly notice that two nondegenerate gapless points are present in the vicinity of the L point. Such gapless points in $\mathbf{k}$ space are called Weyl points or Weyl nodes and unlike Dirac points they are twofold degenerate rather than fourfold. Weyl points (W1) along the $H/2 \rightarrow L \rightarrow H'/2$ direction are located near the Fermi level and are related by TR symmetry (L point as Kramers' point). Hence, these two points have the same chirality and topological charge. Band structure along the $P/2 \rightarrow L \rightarrow Q/2$ direction reveals the presence of two more nondegenerate gapless points located slightly below Fermi level. These two gapless points represent another set of Weyl points depicted by W2. W2 Weyl points are related by TR symmetry and hence, they share the same chirality and topological charge. Even though two Weyl points can be noticed along the $P/2 \rightarrow L \rightarrow Q/2$ direction [Fig. 2(a)], only one Weyl point lies inside the first Brillouin zone. Here, it is worth mentioning that P and Q are not high-symmetry points in the Brillouin zone, and the Q point lies outside of the first Brillouin zone [Fig. 2(c)]. To determine the chirality of the W1 and W2 Weyl points, we have calculated the Berry flux through a closed surface enclosing only one Weyl point at a time [49,50]. Our calculations reveal that W1 and W2 have opposite chirality and therefore, they carry opposite topological charges (see Supplemental Material). Consequently, W1 behaves like a monopole and W2 behaves like an antimonopole in $\mathbf{k}$ space. These two opposite Weyl points are located at different energy values. The existence of such opposite Weyl points, located at different energies, is attributed to the broken I symmetry of the present BiSb system.
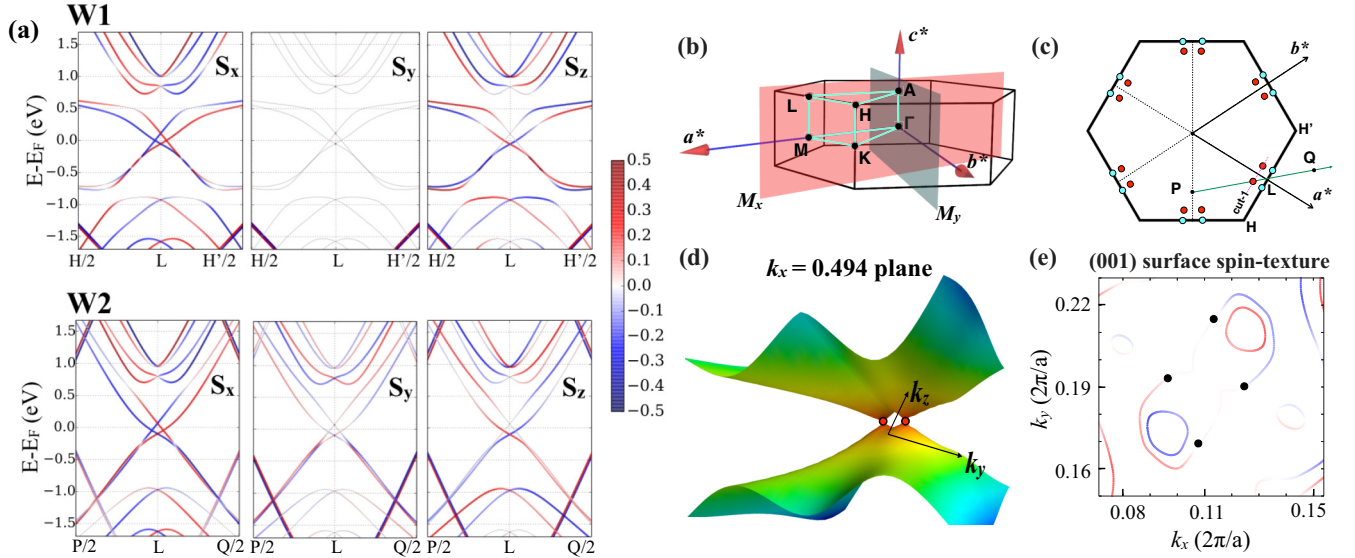
FIG. 2. (a) The spin projections on bands along the $H/2 \rightarrow L \rightarrow H'/2$ (top) and $P/2 \rightarrow L \rightarrow Q/2$ (bottom) directions for 5.0 GPa applied pressure [see (c) for directions in k space]. Red and blue represents projections of up and down spin orientations, respectively (see the color scale). Weyl points along the $H/2 \rightarrow L \rightarrow H'/2$ direction (top) are labeled as W1, while Weyl points along the $P/2 \rightarrow L \rightarrow Q/2$ direction (bottom) are labeled as W2. The **k**-space coordinates of the P and Q points are $(\frac{1}{3}, -\frac{1}{3}, \frac{1}{2})$ and $(\frac{2}{3}, \frac{1}{3}, \frac{1}{2})$, respectively. It is important to notice that W1 Weyl points are located near the Fermi level, however, W2 Weyl points are located slightly below the Fermi level. (c) shows the locations of all Weyl points situated at the $k_z = \frac{\pi}{c}$ plane of the hexagonal Brillouin zone shown in (b). Cyan circles represent W1 Weyl points, while red circles represent W2 Weyl points. (d) shows the dispersion of bands in the $k_x = 0.494$ plane [k_y-k_z plane passing through cut 1 in (c)]. (e) The (001) surface spin texture of BiSb calculated at constant energy $E = 0.10$ eV above Fermi level.

Since W1 and W2 are separated in momentum space as well as in energy, it is impossible to realize a nodal semimetallic phase by tuning the Fermi level and there always exists a state with separate electron and hole Fermi surfaces. Such a property of WSM is very interesting as it could yield chiral magnetic effect and novel topological transport properties in this system. In recent years, these properties have attracted much theoretical interest [6,51–57].

Using the symmetry of the crystal the position of all other Weyl points can be determined. Figure 2(c) shows the location of all Weyl points present at the $k_z = \frac{\pi}{c}$ surface of the hexagonal Brillouin zone. To further confirm the existence of two W2 Weyl points, located slightly away from the high-symmetry line, we calculate the three-dimensional band dispersion at the constant $k_x = 0.494$ plane [see plane along cut 1 in Fig. 2(c)]. Two gapless points can be clearly noticed in Fig. 2(d). In the $R3m$ space group, each type of Weyl point (W1 or W2) gives a total of 12 Weyl points due to the presence of time-reversal, mirror, and C_{3v} rotation symmetries. Thus, in total there are 24 Weyl points in the hexagonal Brillouin zone.

The observation of Fermi arcs connecting two Weyl points is crucial to confirm the prediction of a WSM phase. For this purpose, we have performed the spin-texture calculations at the (001) surface of a BiSb slab [58]. The slab was constructed from the primitive cell of BiSb. We observe two trivial Fermi circles along with two open Fermi curves [Fig. 2(e)]. These open Fermi curves are reminiscent of Fermi arcs connecting opposite Weyl points [59].

Having established the existence of a WSM phase in BiSb, we will finally comment on the possibility to control the

chirality of Weyl points. Here, we take advantage of the large SOC (Bi and Sb atoms are known to exhibit strong SOC [34–36]) and ferroelectric polarization to control the spin-related properties in the present BiSb system.

At zero pressure, the BiSb material is a narrow-band-gap semiconductor which exhibits Rashba-like spin splitting as observed in Fig. 1. In order to quantitatively determine the strength of the Rashba spin splitting at zero pressure, we calculate Rashba energy (E_R) and Rashba parameter (α_R) as described in the corrected version of Ref. [28]. We find that $E_R = 147.3$ meV and $\alpha_R = 10.43$ eV Å for CBB along the L-H direction, while $E_R = 65.9$ meV and $\alpha_R = 4.71$ eV Å for VBT along the L-H direction. Further details about the Rashba spin splitting in this compound can be obtained in Ref. [41]. In the $R3m$ phase, Bi and Sb atoms are displaced from the ideal rocksalt sites. The polar displacement (λ) of the Bi atoms along the direction of red arrows [see crystal structure shown in Fig. 3(a)] yields to a ferroelectric-like polarization in the BiSb system at the semiconducting state. The calculated value of the spontaneous polarization (P^s) at zero pressure is 34.46 μC cm^{-2} (by Berry phase approach [49,60]) and 28.50 μC cm^{-2} (by ionic model). The polarization can be switched by reversing the direction of the polar displacement of Bi atoms from the ideal rocksalt sites [27,28]. We find that the energy barrier (ΔE) to overcome the transition from the paraelectric phase in $R\bar{3}m$ symmetry [41] ($\lambda = 0$) to the ferroelectric phase in $R3m$ symmetry ($\lambda = \pm 1$) is $\Delta E = 0.141$ eV/f.u. (see Supplemental Material, Fig. S5). This energy barrier is comparable with the reported values for other proper ferroelectrics such as BaTiO$_3$ [61], PbTiO$_3$ [61],

(a)

(b)
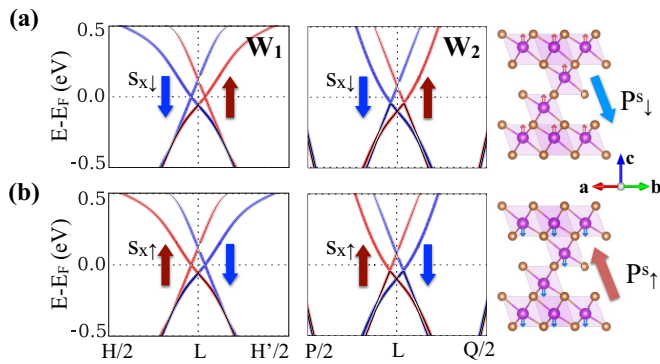
FIG. 3. The spin control and switching of Weyl points by means of polar displacements (P^s) in the system can be observed. (a) [(b)] shows the spin-projected band dispersions near W1 and W2 Weyl points for the original (inverted) polarization cell. The change in the polarization is equivalent to the Bi displacements along up or down directions as shown by the red and blue arrows. Bi and Sb atoms are shown in violet and orange, respectively.

and LiNbO$_3$ [62] and the geometric ferroelectrics BaMgF$_4$ and BaZnF$_4$ [63], in which reported ΔE is 0.018, 0.200, 0.259, 0.133, and 0.218 eV/f.u., respectively. Therefore, we expect ferroelectric switching to be experimentally feasible in the BiSb compound.

We notice that the spin polarization of all three spin components of Rashba-like bands gets inverted when we switch the direction of the ferroelectric polarization at the semiconducting phase at zero pressure. This, as expected from the ferroelectric and SOC coupling terms in the Rashba Hamiltonian [64], makes BiSb (in the $R3m$ phase) a FERSC material at ambient conditions. After the polarization inversion process, we apply isotropic pressure of 4.0 GPa to reach the WSM phase with inverted spin-polarized bands. Figure 3 shows the dispersion of bands along the W1 and W2 Weyl points for the original and inverted polarization cases. The shape of bands and the location of Weyl points in energy and momentum space is exactly the same for both $P^s_\uparrow$ and $P^s_\downarrow$ polarizations. However, after inverting the polarization we found that the spin projection on the bands changes

in spin orientation which is depicted by switching of the up and down S_x spin components (Fig. 3). We observed similar behavior for the S_y and S_z band spin projections. The band spin switching happens along both k directions containing W1 and W2 Weyl points after the polarization is reversed and 4.0 GPa pressure has been applied. As a result, the topological charge and chirality of Weyl points attain opposite values after inverting polarization. This observation suggests the possibility of switching of the monopole and antimonopole charges in a WSM via an electric field. Here, it is important to remark that the WSM phase will retain the polarlike displacements similar to the case of "ferroelectric metals" [31].

In summary, we report a stoichiometric layered structure of BiSb which is enthalpically, vibrationally, and mechanically stable at the DFT level. This structure has a bulk insulating gap at zero pressure with nontrivial band topology. Pressure dependent electronic band structure calculations reveal the existence of a WSM phase in the pressure range 4.0–6.0 GPa. We have found 12 pairs of Weyl points in the first Brillouin zone. Surface state calculations confirm the presence of a WSM phase in BiSb. We further discussed the possibility to control the chirality and topological charge of the Weyl points by means of applied pressure and electric field. The existence of a polarlike Weyl semimetallic phase in this BiSb compound calls for further studies on the underlying exotic quantum phenomena [32].

[1] X. Wan, A. M. Turner, A. Vishwanath, and S. Y. Savrasov, Phys. Rev. B **83**, 205101 (2011).

[2] L. Balents, Physics **4**, 36 (2011).

[3] A. C. Potter, I. Kimchi, and A. Vishwanath, Nat. Commun. **5**, 5161 (2014).

[4] S.-Y. Xu, C. Liu, S. K. Kushwaha, R. Sankar, J. W. Krizan, I. Belopolski, M. Neupane, G. Bian, N. Alidoust, T.-R. Chang, H.-T. Jeng, C.-Y. Huang, W.-F. Tsai, H. Lin, P. P. Shibayev, F.-C. Chou, R. J. Cava, and M. Z. Hasan, Science **347**, 294 (2015).

[5] G. Xu, H. Weng, Z. Wang, X. Dai, and Z. Fang, Phys. Rev. Lett. **107**, 186806 (2011).

[6] A. A. Zyuzin, S. Wu, and A. A. Burkov, Phys. Rev. B **85**, 165110 (2012).

[7] Z. Wang, H. Weng, Q. Wu, X. Dai, and Z. Fang, Phys. Rev. B **88**, 125427 (2013).

[8] H.-J. Kim, K.-S. Kim, J.-F. Wang, M. Sasaki, N. Satoh, A. Ohnishi, M. Kitaura, M. Yang, and L. Li, Phys. Rev. Lett. **111**, 246603 (2013).

[9] K.-Y. Yang, Y.-M. Lu, and Y. Ran, Phys. Rev. B **84**, 075129 (2011).

[10] A. A. Burkov and L. Balents, Phys. Rev. Lett. **107**, 127205 (2011).

[11] A. A. Burkov, M. D. Hook, and L. Balents, Phys. Rev. B **84**, 235126 (2011).

[12] S. Murakami, New J. Phys. **9**, 356 (2007).

[13] G. B. Halász and L. Balents, Phys. Rev. B **85**, 035103 (2012).

[14] Z. Wang, Y. Sun, X.-Q. Chen, C. Franchini, G. Xu, H. Weng, X. Dai, and Z. Fang, Phys. Rev. B **85**, 195320 (2012).

[15] B. Singh, A. Sharma, H. Lin, M. Z. Hasan, R. Prasad, and A. Bansil, Phys. Rev. B **86**, 115208 (2012).

[16] T. Ojanen, Phys. Rev. B **87**, 245112 (2013).

[17] J. Liu and D. Vanderbilt, Phys. Rev. B **90**, 155316 (2014).

[18] M. Hirayama, R. Okugawa, S. Ishibashi, S. Murakami, and T. Miyake, Phys. Rev. Lett. **114**, 206401 (2015).

[19] H. Weng, C. Fang, Z. Fang, B. A. Bernevig, and X. Dai, Phys. Rev. X **5**, 011029 (2015).

[20] A. A. Soluyanov, D. Gresch, Z. Wang, Q. Wu, M. Troyer, X. Dai, and B. A. Bernevig, Nature (London) **527**, 495 (2015).

[21] S.-M. Huang, S.-Y. Xu, I. Belopolski, C.-C. Lee, G. Chang, T.-R. Chang, B. Wang, N. Alidoust, G. Bian, M. Neupane, D. Sanchez, H. Zheng, H.-T. Jeng, A. Bansil, T. Neupert, H. Lin, and M. Z. Hasan, Proc. Natl. Acad. Sci. USA. **113**, 1180 (2016).

[22] S.-M. Huang, S.-Y. Xu, I. Belopolski, C.-C. Lee, G. Chang, B. Wang, N. Alidoust, G. Bian, M. Neupane, C. Zhang, S. Jia, A. Bansil, H. Lin, and M. Z. Hasan, Nat. Commun. **6**, 7373 (2015).

[23] S.-Y. Xu, I. Belopolski, N. Alidoust, M. Neupane, G. Bian, C. Zhang, R. Sankar, G. Chang, Z. Yuan, C.-C. Lee *et al.*, Science **349**, 613 (2015).

[24] B. Q. Lv, H. M. Weng, B. B. Fu, X. P. Wang, H. Miao, J. Ma, P. Richard, X. C. Huang, L. X. Zhao, G. F. Chen, Z. Fang, X. Dai, T. Qian, and H. Ding, Phys. Rev. X **5**, 031013 (2015).

[25] S.-Y. Xu *et al.*, Nat. Phys. **11**, 748 (2015).

[26] L. Lu, Z. Wang, D. Ye, L. Ran, L. Fu, J. D. Joannopoulos, and M. Soljačić, Science **349**, 622 (2015).

[27] S. Picozzi, Front. Phys. **2**, 10 (2014).

[28] D. Di Sante, P. Barone, R. Bertacco, and S. Picozzi, Adv. Mater. **25**, 509 (2013).

[29] M. Liebmann *et al.*, Adv. Mater. **28**, 560 (2016).

[30] Y. Shi, Y. Guo, X. Wang, A. J. Princep, D. Khalyavin, P. Manuel, Y. Michiue, A. Sato, K. Tsuda, S. Yu, M. Arai, Y. Shirako, M. Akaogi, N. Wang, K. Yamaura, and A. T. Boothroyd, Nat. Mater. **12**, 1024 (2013).

[31] N. A. Benedek and T. Birol, J. Mater. Chem. C **4**, 4000 (2016).

[32] E. Bauer and M. Sigrist, *Non-Centrosymmetric Superconductors: Introduction and Overview* (Springer Science & Business Media, New York, 2012), Vol. 847.

[33] D. Puggioni, G. Giovannetti, M. Capone, and J. M. Rondinelli, Phys. Rev. Lett. **115**, 087202 (2015).

[34] L. E. Díaz-Sánchez, A. H. Romero, and X. Gonze, Phys. Rev. B **76**, 104302 (2007).

[35] L. E. Díaz-Sánchez, A. H. Romero, M. Cardona, R. K. Kremer, and X. Gonze, Phys. Rev. Lett. **99**, 165504 (2007).

[36] J. Serrano, R. K. Kremer, M. Cardona, G. Siegle, L. E. Díaz-Sánchez, and A. H. Romero, Phys. Rev. B **77**, 054303 (2008).

[37] S. Curtarolo, A. N. Kolmogorov, and F. H. Cocks, Calphad **29**, 155 (2005).

[38] M. Z. Hasan and C. L. Kane, Rev. Mod. Phys. **82**, 3045 (2010).

[39] G. Kresse and J. Furthmüller, Phys. Rev. B **54**, 11169 (1996).

[40] G. Kresse and D. Joubert, Phys. Rev. B **59**, 1758 (1999).

[41] S. Singh, W. Ibarra-Hernández, I. Valencia-Jaime, G. Avendaño-Franco, and A. H. Romero, Phys. Chem. Chem. Phys. (2016), doi:10.1039/C6CP05401C.

[42] See Supplemental Material at http://link.aps.org/supplemental/10.1103/PhysRevB.94.161116 for the crystal structure, phonon bandstructure, elastic constants, electronic bandstructure at different applied pressures, double-well potential energy-barrier profile for the ferroelectric switching, the calculation of the topological charge of Weyl points, and the Berry curvature calculations.

[43] J. Dismukes, R. Paff, R. Smith, and R. Ulmer, J. Chem. Eng. Data **13**, 317 (1968).

[44] X. Gonze, J.-M. Beuken, R. Caracas, F. Detraux, M. Fuchs, G.-M. Rignanese, L. Sindic, M. Verstraete, G. Zerah, F. Jollet *et al.*, Comput. Mater. Sci. **25**, 478 (2002).

[45] X. Gonze *et al.*, Z. Kristallogr. **220**, 558 (2005).

[46] X. Gonze, B. Amadon, P.-M. Anglade, J.-M. Beuken, F. Bottin, P. Boulanger, F. Bruneval, D. Caliste, R. Caracas, M. Cote *et al.*, Comput. Phys. Commun. **180**, 2582 (2009).

[47] B. Lenoir *et al.*, in *Proceedings of the 15th International Conference on Thermoelectrics* (IEEE, New York, 1996), pp. 1–13.

[48] R. Okugawa and S. Murakami, Phys. Rev. B **89**, 235315 (2014).

[49] R. D. King-Smith and D. Vanderbilt, Phys. Rev. B **47**, 1651 (1993).

[50] Sinisa Coh *et al.*, PythTB code, 2010, http://www.physics.rutgers.edu/pythtb/about.html.

[51] K. Fukushima, D. E. Kharzeev, and H. J. Warringa, Phys. Rev. D **78**, 074033 (2008).

[52] A. G. Grushin, Phys. Rev. D **86**, 045001 (2012).

[53] V. Aji, Phys. Rev. B **85**, 241101 (2012).

[54] A. A. Zyuzin and A. A. Burkov, Phys. Rev. B **86**, 115133 (2012).

[55] P. Hosur and X. Qi, C. R. Phys. **14**, 857 (2013).

[56] M. M. Vazifeh and M. Franz, Phys. Rev. Lett. **111**, 027201 (2013).

[57] M.-C. Chang and M.-F. Yang, Phys. Rev. B **91**, 115203 (2015).

[58] A. H. Romero and F. Munoz, PyProcar code, 2015, http://sourceforge.net/p/pyprocar/PyPROCAR/HEAD/tree/.

[59] I. Belopolski, S.-Y. Xu, D. S. Sanchez, G. Chang, C. Guo, M. Neupane, H. Zheng, C.-C. Lee, S.-M. Huang, G. Bian, N. Alidoust, T.-R. Chang, B. K. Wang, X. Zhang, A. Bansil, H.-T. Jeng, H. Lin, S. Jia, and M. Z. Hasan, Phys. Rev. Lett. **116**, 066802 (2016).

[60] D. Vanderbilt, J. Phys. Chem. Solids **61**, 147 (2000).

[61] R. E. Cohen, Nature (London) **358**, 136 (1992).

[62] M. Ye and D. Vanderbilt, Phys. Rev. B **93**, 134303 (2016).

[63] M. Núñez Valdez, H. T. Spanke, and N. A. Spaldin, Phys. Rev. B **93**, 064112 (2016).

[64] Y. A. Bychkov and E. I. Rashba, J. Phys. C **17**, 6039 (1984).